Biosensors and Bioelectronics 44 (2013) 1–5

Contents lists available at SciVerse ScienceDirect

Biosensors and Bioelectronics

journal homepage: www.elsevier.com/locate/bios

Innovative biocompatible nanospheres as biomimetic platform for electrochemical glucose biosensor

Wenbo Zhao [a,1], Yalong Ni [a,1], Qinshu Zhu [a], Rongjin Fu [c], Xiaohua Huang [a,*], Jian Shen [a,b,**]

[a] Jiangsu Key Laboratory of Biofunctional Materials, College of Chemistry and Materials Science, Nanjing Normal University, Nanjing 210023, PR China
[b] Research Center of Surface and Interface Chemistry and Engineering Technology, Nanjing University, Nanjing 210093, PR China
[c] Nanjing Institute of Supervision and Testing on Product Quality, Nanjing 210028, PR China

ARTICLE INFO

Article history:
Received 16 November 2012
Received in revised form
16 December 2012
Accepted 17 December 2012
Available online 9 January 2013

Keywords:
Silica
Phytic acid
Biomimetic
Glucose oxidase
Biosensor

ABSTRACT

In this work, the silica– phytic acid (SiO_2–PA) nanocomposites were synthesized by the method of reverse microemulsion and electrostatic binding. The newly designed materials were used to develop a novel glucose biosensor by immobilizing glucose oxidase (GO*x*) onto the SiO_2–PA nanocomposites film on the surface of glassy carbon electrode (GCE). The characteristics of SiO_2–PA nanocomposites and GO*x* were obtained by using transmission electron microscopy (TEM), Fourier transform infrared (FTIR) spectroscopy and circular dichroism (CD) technique. All the results indicated that silica nanoparticales were modified with phosphate radicals successfully and the biomimetic surface was built. The entrapped GO*x* could preserve its bioactivity and exhibited an excellent electrochemical behavior with a formal potential of −0.548 V in phosphate buffer solution (PBS) (pH=7). Response studies to glucose were carried out using differential pulse voltammetry (DPV). The results indicated that the modified electrode can be used to determine glucose without interference from L-ascorbic acid (AA) and uric acid (UA) with the low detection limit of 0.012 mM. The comparison tests of DPVs of different electrodes in the absence and presence of glucose were also studied. The biosensor can also be used for quantification of the concentration of glucose in real samples.

1. Introduction

With the development of nanotechnology in recent years, a lot of novel nanomaterials have been fabricated and the applications in biosensors have also advanced greatly (Zhang et al., 2009; Pan et al., 2008; Cui, 2007). Nanomaterials possess unique advantages over other conventional materials in terms of enzymatic immobilization because of their high surface to volume ratios and high surface activity (Zhao et al., 2010; Tian et al., 2002; Rodriguez et al., 2000). But the conductivity and biocompatibility of nanomaterials are the key issues to be resolved because these two characteristics usually cannot be offered simultaneously for general nanomaterials.

The metal nanoparticles (Me-NPs) have recently become important as modified materials of electrode for their good electrical conductivity. We rarely encountered biosensor which is modified with Me-NPs solely due to the unsatisfactory biocompatibility of Me-NPs. The biological activity and native secondary structure of enzyme cannot be preserved because of the effect of metal surface induced denaturation. So some composite materials which contain Me-NPs were used to make biosensors, for example, Hb/Au-F127 nanospheres/GCE (Ni et al., 2012), hemoglobin/silver nanoparticle/hyaluronan multilayer (Zhang et al., 2012a) and Hb/gold nanoparticles/polythionine/platinum nanoparticles/GCE (Zhang et al., 2012b). The problem of proteins denaturation can be solved by using biocompatible polymeric nanoparticles for immobilization on electrode surface. Their good biocompatibility can provide the desirable microenvironment to proteins. However, good conditions cannot be created for the fast electron transfer between the protein and the underlying electrode for most polymers owing to their weak or extremely low conductivity. Therefore, they usually get help from carbon materials to construct sensors such as GO*x*/silica gel/multiwalled carbon nanotubes/polyacrylonitrile/GCE (Nenkova et al., 2010), tyrosinase-chitosan-CNi/GCE (Yang et al., 2012) and Hb/polyurethane ionomer/multiwalled carbon nanotubes/GCE (Zhao et al., 2011).

Among inorganic nanomaterials, silica has attracted much attention due to its low toxicity, easy preparation and low cost. However, recent studies have shown that different silica particles

* Corresponding author.
** Corresponding author at: Jiangsu Key Laboratory of Biofunctional Materials, College of Chemistry and Materials Science, Nanjing Normal University, Nanjing 210023, PR China. Tel.: +86 25 85891651; fax: +86 25 83598280.
E-mail addresses: huangxiaohua@njnu.edu.cn (X. Huang), shenjian@nju.edu.cn (J. Shen).
[1] These two authors made equal contribution to this paper.

0956-5663/$ - see front matter © 2013 Published by Elsevier B.V.
http://dx.doi.org/10.1016/j.bios.2012.12.036

can cause different extent of cytotoxicity. Results obtained from Kim's group have demonstrated that non-porous silica nanoparticle and colloidal silica can induce in vitro cytotoxicity and inflammation (Kim et al., 2011). Gao and his partners presented their study that the adhesion and migration ability of the fibroblasts were impaired by silica particles regardless of their size (Zhang et al., 2010).

Phytic acid (PA), also known as inositol hexakisphosphoric acid, and its salts are small molecules with six phosphates groups (Fig. 1S) (Samba-Fouala et al., 2000). PA is a naturally derived material from legume seeds, cereal grains, beans and animal hematid. It is biocompatible, nontoxic, current conducting and green environmental (Jo et al., 2008). Owing to its six phosphates groups, PA has a strong tendency to combine or interact with positively charged materials or groups. Assembled layer-by-layer films of PA with other materials such as poly(allylamine hydrochloride) (Tang et al., 2010), mesoporous gold film (Wang et al., 2010) and TiO_2 (McKenzie and Marken, 2003) were reported. Some biosensors based on phytic acid have also been investigated. The direct electrochemistry of cytochrome c based on TiO_2 phytate film nanocomposite was reported by McKenzie et al. (2005). Chen's group developed a novel stable H_2O_2 biosensor based on $(Fe_3O_4$/chitosan–phytic acid$)_n$ films which can keep Hb's high catalytic activity towards many substances (Zhao et al., 2006).

Phosphate buffer is one of the main buffer in the system of life. In addition, the functional P–O bond is an important component of phospholipid in the cell membrane. So adding the P–O bond (phosphates group) into biomaterials can be viewed as bionic building to improve the biocompatibility of general materials (Alferiev et al., 2001; Adhikari et al., 2008). So far no study has yet reported on the synthesis of silica modified with phytic acid. Herein, SiO_2–PA ionomer nanoparticles were synthesized based on electrostatic interaction between PA and SiO_2 that was pretreated with (3-aminopropyl) triethoxysilane (APTES) and then SiO_2–PA nanospheres were successfully immobilized on GCE. Glucose oxidase was chosen as a model protein and the direct electrochemistry of GO*x* was investigated. More details were presented.

2. Experimental

2.1. Reagents

Triton X-100, (3-Aminopropyl) triethoxysilane (APTES, 98 wt%), phytic acid (PA, 70 wt%) solution and phytic acid sodium salt hydrate ($\geq$98 wt%) were purchased from Aladdin Chemistry Co. Ltd., tetraethyl orthosilicate (TEOS, $\geq$28.4 wt%) was purchased from Sinopharm Chemical Reagent Co. Ltd., GO*x* was obtained from Sigma-Aldrich Co., β–D-(+)-glucose (99%) was from J&K Chemical Co. Inc., and cyclohexane, hexanol, aqueous ammonia solution ($NH_3 \cdot H_2O$, 71 wt%) were obtained from Shanghai Lingfeng Chemical Reagent Co. Ltd.. Phosphate buffer solution was prepared by mixing stock standard solution of Na_2HPO_4 and NaH_2PO_4. All solutions were made up with twice-distilled water and all chemicals and solvents were of analytical grade.

2.2. Preparation of SiO_2–PA nanoparticles

Silica nanoparticles (SiO_2 NPs) were synthesized using a water-in-oil (W/O) or reverse microemulsion method. The detailed preparation process was described in previous paper. (Bagwe et al., 2006). SiO_2 NPs were collected by centrifugation at 3000 rpm for 15 min and washed three times with ethanol and twice-distilled water, respectively. 0.25 g SiO_2 NPs were redispersed into 100 mL deionized water and followed by the addition of 500 μL TEOS for particle post-coating, the mixture was allowed to stir for 0.5 h. The silica surface was substituted with amino groups by reaction with 500 μL APTES. Then, 600 μL phytic acid solution (the pH value was adjusted to 7 by phytic acid sodium salt hydrate) was added into the mixture at room temperature and allowed to stir for 24 h. Finally, PA-functionalized silica nanoparticles were centrifuged, washed with ethanol and twice-distilled water, dried at 60 °C for 24 h under vacuum.

2.3. Construction of the GOx/(SiO_2–PA)/GCE

Prior to the modification, GCE was mechanically polished with wetted microcloth containing 0.3 and 0.05 μm alumina powder, and then carefully cleaned in ethanol and water by ultrasonication bath for 5 min, the GCE was allowed to dry at room temperature. 2 mg of SiO_2–PA was dispersed into 4 mL PBS to obtain a suspension of 0.5 mg mL^{-1} SiO_2–PA. 6.0 μL of the resulting SiO_2–PA solution was dropped onto the electrode surface and dried in air. Then, 6.0 μL of 1.5 mg mL^{-1} GO*x* solution in 0.1 M PBS (pH=7.0) was dropped onto the surface of (SiO_2–PA)/GCE and allowed to dry at ambient temperature to obtain the GO*x*/(SiO_2–PA)-modified electrode. Finally, 4 μL of Nafion (1%) was cast on the GO*x*/(SiO_2–PA)-modified electrode surface and the GO*x*/(SiO_2–PA)/Nafion-modified electrode was obtained. The same modified method was used to fabricate other modified electrodes. The obtained modified electrodes were stored at 4 °C in a refrigerator when not in use.

2.4. Apparatus and measurements

Transmission electron microscopy (TEM) images were obtained using an interface high-resolution transmission electron microscopy (HITACHI H-7650, Japan). The FTIR spectra of SiO_2, PA and SiO_2–PA were measured using a Cary 5000 Fourier transform infrared spectrophotometer (VARIAN Company). The Circular dichroism (CD) spectra in the far-UV (with the range from 200 to 260 nm) were measured on a JASCO J-715 spectropolarimeter using a 1 cm quartz cuvette. The contents of α-helix, β-sheet, β-turn and the random coil conformation were calculated using the JASCO710 program. All electrochemical experiments were performed on a CHI 760C electrochemical analyzer (CHInstruments, Inc., US), using a conventional three-electrode system with a GCE (3 mm in diameter, Shanghai Chenhua, China) as the working electrode, a platinum wire as the auxiliary electrode and a saturated calomel electrode (SCE) as the reference electrode. Cyclic voltammogram experiments were carried out in quiescent solution at 100 mV s^{-1} in 5 mL of 0.1 M PBS, and the solution was purged with high purity nitrogen firstly and blanked with nitrogen during the electrochemical experiments. DPV measurements were carried out with pulse amplitude of 0.05 V and pulse width of 0.2 s.

3. Results and discussion

3.1. Characterization of the SiO_2–PA nanocomposites and GOx/(SiO_2–PA) nanocomposites film

TEM images of SiO_2 and SiO_2–PA nanocomposites that were presented in Fig. 1 showed SiO_2–PA nanoparticles consisting of extremely monodispersed elliptic nanoparticles (Fig. 1b) with the average diameter of 50 nm while SiO_2 NPs were slightly agglomerated (Fig. 1a). The size of SiO_2 NPs modified with PA did not change considerably, taking the simple SiO_2 NPs as the reference.

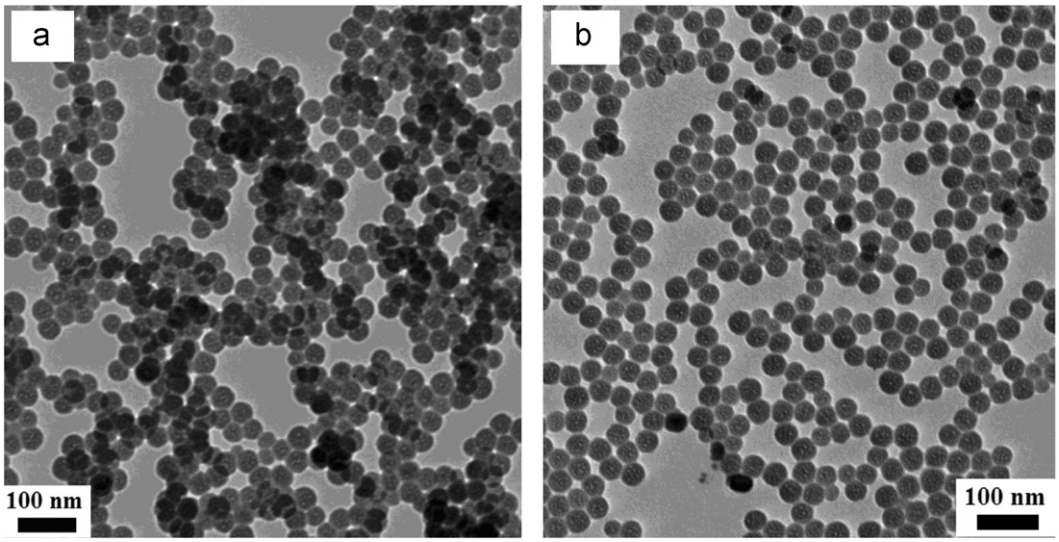

Fig. 1. TEM images of SiO_2 (a) and SiO_2–PA (b).

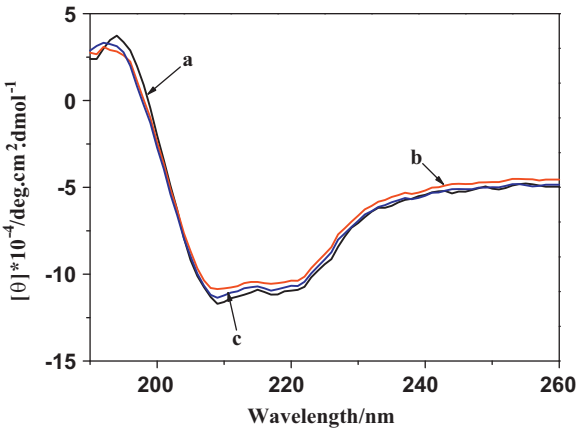

Fig. 2. CD spectra of pure GO*x* (a), GO*x*/SiO_2 (b) and GO*x*/(SiO_2–PA) (c) in 0.1 M PBS (pH=7.0) in the wavelength region of 190–260 nm.

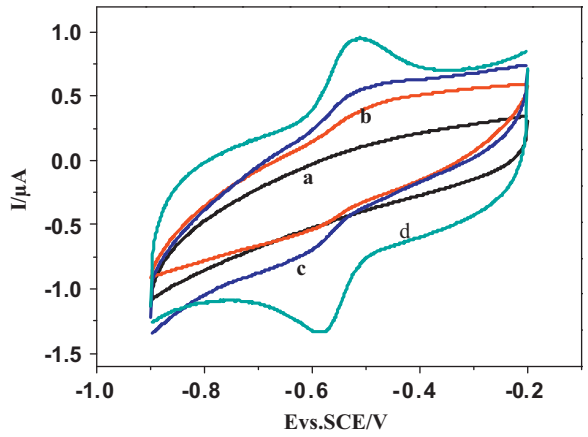

Fig. 3. Cyclic voltammograms of (SiO_2–PA)/GCE (a), GO*x*/GCE (b), GO*x*/SiO_2/GCE (c) and GO*x*/(SiO_2–PA)/GCE (d) in 0.1 M PBS (pH=7.0). Scan rate: 100 mV s^{-1}.

FTIR spectra of SiO_2, PA and SiO_2–PA composites are represented in Fig. 2S. The spectrum of SiO_2 showed two broad bands around 1110, 973 cm^{-1} attributed to asymmetric O–Si–O stretching and a weak peak at 1620 cm^{-1} which was ascribed to the bending vibrations of water molecule (curve a). The bands of the phosphate group at 1104 and 1250 cm^{-1} were observed in the spectrum of PA powder (curve b). In the spectrum of SiO_2–PA (curve c), the superfluous peaks at 2927, 1560 and 693 cm^{-1} attributed, respectively to –C-NH_2 stretching, symmetric –NH_2 stretching and the bending vibrations of –NH, which indicated the successful combination of SiO_2 and APTES. In addition, the phosphate bands at 1104 cm^{-1} are intense and overlap the O–Si–O bands.

Circular dichroism is a quite suitable tool to estimate the secondary structure content of proteins (Wu et al., 2008). In the far-UV region (190–260 nm), the spectrum which corresponds to the peptide $n \rightarrow \pi^*$ electronic transition was sensitive to the conformation of the secondary structure of GO*x* (Zoldák et al., 2004). Fig. 2 displayed the CD spectra of GO*x*, GO*x*/SiO_2 and GO*x*/(SiO_2–PA). The CD spectrum of GO*x*/(SiO_2–PA) were characterized by two negative bands at around 208 and 219 nm (curve c) which looks very similar to that of the pure GO*x* (curve a) in both peak intensity and peak position, while GO*x*/SiO_2 caused slightly larger difference (curve b) compared with the native one. In addition, the contents of α-helix and β-turn conformation of GO*x*/(SiO_2–PA) increased by 0.7 and 0.5%, respectively, while GO*x*/SiO_2 changed 2.3 and 3.2% compared with pure GO*x*. All results indicated that SiO_2–PA nanocomposites could essentially maintain the native conformation of GO*x*. Thus, the secondary structure of GO*x* was well maintained in the prepared biosensor and SiO_2–PA nanocomposites indeed have good biocompatibility.

3.2. Direct electrochemistry of the GO*x*/(SiO_2–PA)/GCE

In order to investigate the electrochemical properties of GO*x*/(SiO_2–PA)/GCE, different modified electrodes were tested using cyclic voltammetry. Fig. 3 showed the CVs of different electrodes in 0.1 M PBS (pH=7.0) at a scan rate of 100 mV s^{-1}. No voltammetric signal was observed at SiO_2–PA film electrode (curve a) while GO*x*/GCE gave a weak voltammetric signal in the range of -0.9 to −0.2 V (curve b). Comparing with GO*x*/SiO_2/GCE (curve c), GO*x*/(SiO_2–PA)/GCE displayed a pair of well-defined and quasi-reversible CV peaks with a formal potential value ($E^{0'}$) of −0.548 V (curve d). The current signal of the redox peaks at GO*x*/(SiO_2–PA) film were larger than that of no PA. The good electrochemical response of GO*x*/(SiO_2–PA)/GCE indicated that SiO_2–PA played an important role in facilitating the electron exchange between the electroactive center of GO*x* and GCE. In

addition, the nanocomposites provided a mild environment so that the bioactivity of GO*x* can be retained.

The influence of scan rate on direct electrochemistry of the immobilized GO*x* was investigated in Fig. 3S(A). When the scan rate increased from 20 to 300 mV s^{-1}, the anodic peak potential of GO*x* shifted to a more positive value and the cathodic peak potential shifted in a negative direction. The good stability of GO*x*/(SiO_2–PA)/GCE was shown in the inset of Fig. 3S(A). At the same time, the redox peak current increased linearly with linear regression equations as I_{pa} (mA)=0.1479+0.00279ν (mV s^{-1}) (r=0.994) and I_{pc} (mA)=−0.1562–0.00273ν (mV s^{-1}) (r=0.993) (Fig. 3S(B)). The results suggested that the redox reaction of GO*x* on the SiO_2–PA film modified electrode is a quasi-reversible surface-controlled electrochemical process. The electron transfer rate constant (k_s) value of the GO*x* on the modified film was calculated to be 2.25 s^{-1} using the Laviron's (1979) equations, which was larger than those data obtained for GO*x* immobilized on MWCNTs-chitosan (1.08 s^{-1}) (Luo et al., 2006), boron-doped MWCNTs (1.56 s^{-1}) (Deng et al., 2008). Such results revealed a reasonably fast electron transfer between the redox center of the enzyme and the electrode surface.

As shown in Fig. 4S(A), the pH value of the solution had an effect on the electrochemical behavior of GO*x* on the SiO_2–PA film. A negative shift of both the cathodic and anodic peak potentials occurs when the solution pH value was increased, and the maximum peak currents of GO*x* occurred at pH 7.0 which was chosen in our follow-up work. The redox potential $E^{0'}$ changes linearly as a function of solution pH from 5.5 to 7.5 with a slope of −52 mV pH^{-1} (Fig. 4S(B)), which was close to the theoretical value of −58.6 mV pH^{-1} (Liu et al., 2007), indicating two protons and two electrons were involved in the electron transfer process.

3.3. Electrocatalysis of GOx/(SiO_2–PA)/GCE to glucose

The DPV studies of GO*x*/(SiO_2–PA)/GCE were carried out in PBS buffer (pH=7.0) in the voltage range from −0.8 to −0.3 V (Fig. 4A). Moderate stirring was kept for about 1 min when glucose solution was successively added to the buffer solution prior to recording the DPV voltammograms. An apparent peak was observed at −0.548 V and the peak current gradually increased with the increasing concentration of glucose. The calibration curve was presented in Fig. 4B. The peak current showed a linear increase with the range of glucose concentration from 0.016 to 8 mM and the calculated detection limit was 0.012 mM. The detection performance of the proposed biosensor was compared with that of other methods as shown in Table 1S. GO*x*/(SiO_2–PA)/GCE exhibited excellent performance in terms of a wider linear range and lower limit of detection for glucose. Such results may be due to the good biocompatibility and the favorable electrical conductivity of PA. Biomimetic surface of SiO_2–PA provided a friendly microenvironment to retain GO*x*'s bioactivity. The DPVs of other electrodes were displayed in Fig. 5S and more detailed explanation were presented in supplementary material. The other analytical characteristics of the biosensor were evaluated. The relative standard deviation (RSD) was 1.7% for ten different and freshly prepared electrodes, revealing an acceptable reproducibility of the electrode. The stability of the electrode was also good after 30 days' storage at 4 °C (> 93%), and it still retained around 80% of initial response after 60 days.

3.4. Anti-interference properties of GOx/(SiO_2–PA)/GCE biosensor

AA and UA are coexisting electroactive species in real samples which might affect the biosensors response. The anti-interference advantages of the biosensor were displayed in Fig. 5. Only one clear peak can be observed in the presence of UA (curve a), which

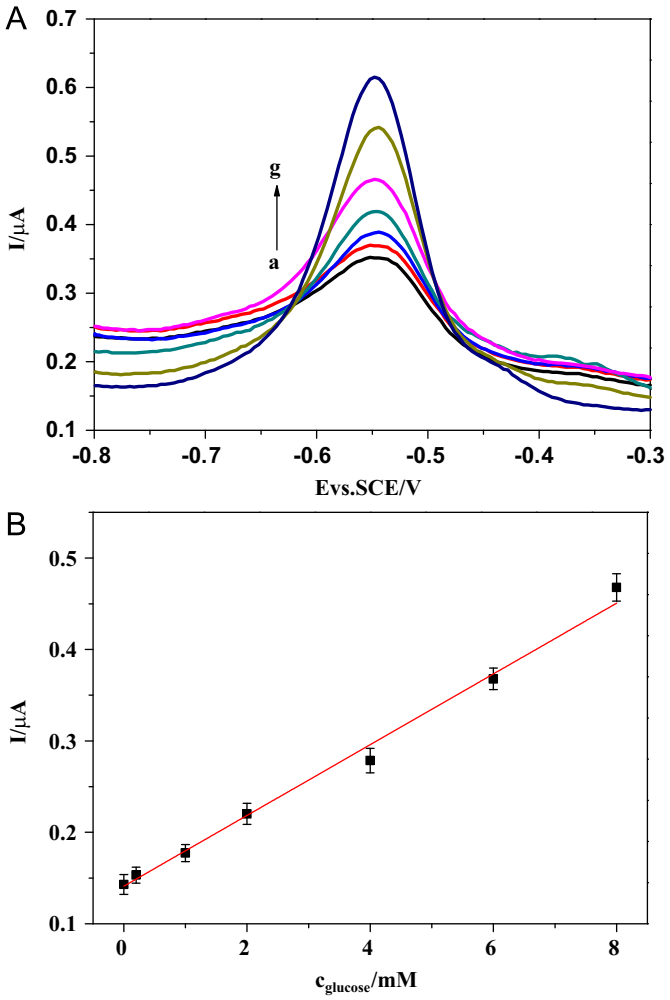

Fig. 4. (A) DPVs obtained at GO*x*/(SiO_2–PA)/GCE in 0.1 M PBS (pH=7.0) with the concentration of glucose (from a to g) 0, 0.2, 1, 2, 4, 6, 8 mM. (B) Relationship between the peak current and the concentration of glucose.

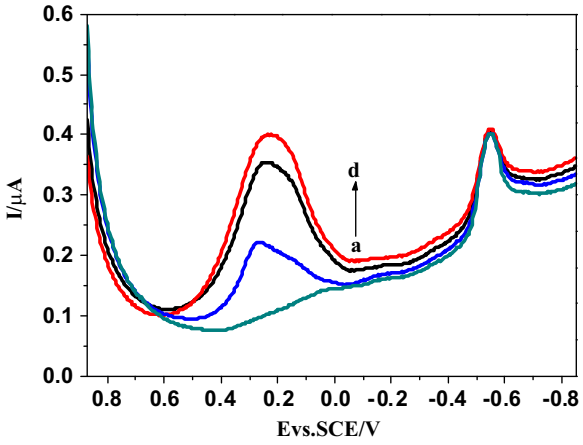

Fig. 5. DPVs for 1 mM glucose in the presence of 1 mM UA (a), 1 mM UA and 1 mM AA (b), 10 mM UA and 10 mM AA (c), 20 mM UA and 20 mM AA (d) at the GO*x*/(SiO_2–PA)/GCE in 0.1 M PBS (pH=7).

indicated that the electrode did not respond to UA. Curve b presented two distinct peaks in the presence of UA and AA, obviously, the peak at the potential of 0.24 V attributed to the presence of AA. In addition, with the increasing concentration of UA and AA (curves c and d), there were no other peaks observed,

Table 1
Determination of glucose content in real sample using the GO*x*/(SiO_2–PA)/GCE biosensor.

Sample	Referenced Values[a](mM)	Determined values[b](mM)	Relative deviation (%)
Bovine serum	4.4	4.27 ± 0.32	−2.9
Mouse blood	3.6	3.71 ± 0.39	3.1
Rabbit blood	19.9	16.2 ± 1.96	−18.6
Human blood	3.5	3.46 ± 0.25	−1.1

[a] Value provided by the hospital.
[b] Value determined by the GO*x*/(SiO_2–PA)/GCE biosensor.

and the response to AA was correspondingly increasing while the peak currents of glucose were fairly stable. All the results suggested that the electroactive species UA and AA can not interfere with the response to glucose of the electrode even if the concentration of interferents was large from 1 to 20 mM. Thereby, we can conclude that the resulting biosensor has a strong anti-interference ability.

3.5. Real sample analysis

The biosensor was further applied to determine the glucose content in bovine serum, mouse blood, rabbit blood and human blood samples. The samples were diluted with PBS by 5 times before detection. As shown in Table 1, the values measured by the proposed biosensor were in good agreement with the data provided by hospital except the rabbit blood. The possible reason was that the blood glucose concentration of rabbit exceeded the detection range of this biosensor. All the results demonstrated that the proposed biosensor was reliable and sensitive for the determination of glucose.

4. Conclusion

The SiO_2–PA nanocomposites were synthesized by the method of reverse microemulsion and electrostatic binding, and used to construct a novel glucose biosensor. The result of CD spectra indicated that the protein on SiO_2–PA film retained near-native secondary structures. The biocompatibility of SiO_2 NPs which modified with PA was excellent. The proposed biosensor also displayed good electrocatalytical activity to glucose. The biomimetic surface of SiO_2–PA nanoparticles played an important role to the superior properties of the resulting biosensor. The satisfying results for real sample analysis indicated that the biosensor we prepared had a great potential for practical application.

Acknowledgments

The work was supported by NSFC (21144002, 20971069), NSFJS (BK2011781), The Natural Science Key Basic Research Foundation of the Jiangsu Higher Education Institutions of China (11KJB150009, 12KJA150006). the Project Funded by the Priority Academic Program Development of Jiangsu Higher Education Institutions, and Base of production, education & research of prospective joint research project of Jiangsu Province (BY2011109).

Appendix A. Supporting information

Supplementary data associated with this article can be found in the online version at http://dx.doi.org/10.1016/j.bios.2012.12.036.

References

Adhikari, R., Gunatillake, P.A., Griffiths, I., Tatai, L., Wickramaratna, M., Houshyar, S., Moore, T., Mayadunne, R., Field, J., McGee, M., 2008. Biomaterials 29, 3762–3770.
Alferiev, I., Vyavahare, N., Song, C., Connolly, J., Travis Hinson, J., Lu, Z., Tallapragada, S., Bianco, R., Levy, R., 2001. Biomaterials 22, 2683–2693.
Bagwe, R.P., Hilliard, L.R., Tan, W., 2006. Langmuir 22, 4357–4362.
Cui, D., 2007. Journal of Nanoscience and Nanotechnology 74, 1298–1314.
Deng, C., Chen, J., Chen, X., Xiao, C., Nie, L., Yao, S., 2008. Biosensors and Bioelectronics 23, 1272–1277.
Jo, S., Jeong, H., Bae, S.R., Jeon, S., 2008. Microchemical Journal 88, 1–6.
Kim, D., Lin, Y.S., Haynes, C.L., 2011. Analytical Chemistry 83, 8377–8382.
Laviron, E., 1979. Journal of Electroanalytical Chemistry and Interfacial Electrochemistry 101, 19–28.
Liu, Q., Lu, X., Li, J., Yao, X., 2007. Biosensors and Bioelectronics 22, 3203–3209.
Luo, X., Killard, A.J., Smyth, M.R., 2006. Electroanalysis 18, 1131–1134.
McKenzie, K.J., Marken, F., 2003. Langmuir 19, 4327–4331.
McKenzie, K.J., Marken, F., Opallo, M., 2005. Bioelectrochemistry 66, 41–47.
Nenkova, R., Ivanova, D., Vladimirova, J., Godjevargova, T., 2010. Sensors and Actuators B: Chemical 148, 59–65.
Ni, Y., Wang, Y., Zhang, G., Shen, J., Zhao, W., Huang, X., 2012. Electrochimica Acta 69, 282–286.
Pan, B., Cui, D., Ozkan, C.S., Ozkan, M., Xu, P., Huang, T., Liu, F., Chen, H., Li, Q., He, R., 2008. The Journal of Physical Chemistry C 112, 939–944.
Rodriguez, J.A., Jirsak, T., Dvorak, J., Sambasivan, S., Fischer, D., 2000. The Journal of Physical Chemistry B 104, 319–328.
Samba-Fouala, C., Mossoyan, J.C., Mossoyan-Déneux, M., Benlian, D., Chanéac, C., Babonneau, F., 2000. Journal of Materials Chemistry 10, 387–393.
Tang, F., Wang, X., Xu, X., Li, L., 2010. Colloids and Surfaces A: Physicochemical and Engineering Aspects 369, 101–105.
Tian, Z.R., Voigt, J.A., Liu, J., Mckenzie, B., Mcdermott, M.J., 2002. Journal of the American Chemical Society 124, 12954–12955.
Wang, Y., Ma, X.L., Wen, Y., Zheng, Y.Q., Duan, G.P., Zhang, Z.R., Yangz, H.F., 2010. Journal of the Electrochemical Society 157, K5–K9.
Wu, X., Du, P., Wu, P., Cai, C., 2008. Electrochimica Acta 54, 738–743.
Yang, L., Xiong, H., Zhang, X., Wang, S., 2012. Bioelectrochemistry 84, 44–48.
Zhang, F., Wu, J., Zhang, H., 2012a. Journal of Solid State Electrochemistry 16, 1683–1692.
Zhang, X., Guo, Q., Cui, D., 2009. Sensors 9, 1033–1053.
Zhang, Y., Hu, L., Yu, D., Gao, C., 2010. Biomaterials 31, 8465–8474.
Zhang, Y., Yuan, R., Chai, Y., Wang, J., Zhong, H., 2012b. Journal of Chemical Technology and Biotechnology 87, 570–574.
Zhao, G., Xu, J.J., Chen, H.Y., 2006. Electrochemistry Communications 8, 148–154.
Zhao, W., Zhang, G., Jiang, L., Lu, T., Huang, X., Shen, J., 2011. Colloids and Surfaces B: Biointerfaces 88, 78–84.
Zhao, Z., Lei, W., Zhang, X., Wang, B., Jiang, H., 2010. Sensors 10, 1216–1231.
Zoldák, G., Zubrik, A., Musatov, A., Stupák, M., Sedlák, E., 2004. Journal of Biological Chemistry 279, 47601–47609.